

High-resolution Fourier-transform spectroscopy of solid parahydrogen in the first overtone region

Markus Mengel, Brenda P. Winnewisser, and Manfred Winnewisser

Physikalisch-Chemisches Institut, Justus-Liebig-Universität Giessen, Heinrich-Buff-Ring 58, D-35392 Giessen, Germany

(Received 3 September 1996)

The first vibrational overtone spectrum of solid parahydrogen with various low orthohydrogen impurity levels has been studied in the range 7900–10 000 cm^{-1} using a White-type external multireflection system with a 34.8-cm sample path length. We were able to detect extremely weak features, namely, the $Y_1(0)$ at 7991.85 (1) cm^{-1} , and the double transitions $U_1(0) + Q_1(1)$, $U_1(0) + S_1(0)$, $U_1(1) + Q_1(0)$, and $Q_1(0) + Q_1(0)$. The $Q_1(0) + Q_1(1)$ and $Q_1(1) + Q_1(1)$ double transitions were resolved. We obtained a rich orthohydrogen satellite spectrum associated with the transitions $Q_2(0)$ and $Q_2(1)$ near 8060 cm^{-1} . An analysis and assignment of these satellite transitions are presented. The double transitions of the type $Q_1(J) + Q_1(J')$ ($J, J' = 0, 1$) are located in the spectral region around 8300 cm^{-1} . The most remarkable features here are the $Q_1(1) + Q_1(1)$ transition, which consists entirely of fine structure, and the $Q_1(0) + Q_1(0)$ transition, which, to our knowledge, has an intensity that cannot be accounted for by previously proposed mechanisms. Finally the thermal shift of all of the above-mentioned transitions was investigated by lowering the sample temperature from 12.5 K down to 6.5 K while taking spectra. The influence of the change of temperature on the line positions, linewidths, and interaction parameters of solid hydrogen is discussed. [S0163-1829(97)07215-9]

I. INTRODUCTION

Solid hydrogen has drawn the attention of spectroscopists for many years because it constitutes the only molecular crystal in which the molecules retain their gas phase properties of rotation and vibration. In addition, it is possible to study solid-state effects and intermolecular forces between these simplest of all molecules in the infrared and Raman spectra of solid hydrogen. One of the most important consequences of intermolecular forces is the fact that infrared transitions that are completely forbidden for isolated molecules become allowed in the solid and can lead to surprisingly strong absorption features. In solid hydrogen we observe rotational transitions with $\Delta J=0$, labeled with Q , $\Delta J=2$ (S), $\Delta J=4$ (U), $\Delta J=6$ (W), and even $\Delta J=8$ (Y); we recently reported the observation of the $Y_0(0)$ transition.¹ The subscript indicates the vibrational quantum number of the upper state; the lower state always has $v=0$ for absorption spectra. The number in parentheses is the J value of the lower state. Vibrational transitions have been observed up to the third vibrational overtone region ($v=4$).² Another result of the intermolecular induction mechanisms is that two neighboring hydrogen molecules can be excited simultaneously upon absorption of only one photon, in so-called double transitions.

The pure rotational transitions and the fundamental band of solid H_2 and D_2 have been extensively studied.³⁻⁷ Recently high-resolution spectra of the second overtone region have been reported.^{8,9} The interpretation and analysis of these spectra have relied on the theoretical approach developed by Van Kranendonk and co-workers.¹⁰⁻¹³ Investigations of the first overtone region of solid hydrogen at various orthohydrogen impurity levels have been previously reported in several publications. The important work of Varghese, Prasad, and Reddy¹⁴ covered the wave number region 8000–

9400 cm^{-1} , however, with a relatively low resolution of 4 cm^{-1} using a grating spectrometer. The work of Lee¹⁵ covered the same region at a resolution of 0.4 cm^{-1} . Oka and co-workers⁸ made the first observation of the internal structure of the $Q_2(0)$ transition in this region with a resolution of 0.1 cm^{-1} , showing a twofold splitting due to crystal-field interactions. The purpose of the present work was to investigate the first-overtone region of solid parahydrogen with high resolution, high sensitivity, and low orthohydrogen impurity levels using a Bruker IFS 120 HR Fourier-transform spectrometer. We particularly aimed at recording satellite spectra of the $Q_2(J)$ transitions due to the orthohydrogen pair interaction and the $Q_1(J)+Q_1(J')$ double transitions. These spectra and other new spectral features are presented here.

II. EXPERIMENTAL SETUP

The experimental setup was a modification of the experiment described in detail in our previous publications.^{1,7,16} We used an external multireflection system (White type cell) in which the number of passes through the cell within the liquid-He vaporization cryostat (Janis Research Inc., Model 10 DT) was increased from 4 to 8. This multireflection system was mounted inside the sample chamber of the Bruker IFS 120 HR interferometer as shown in Fig. 2 of Ref. 16. Water absorptions were minimized by evacuating the whole spectrometer. All six windows of the cryostat and of the sample cell were equipped with an antireflection coating, which was optimized for the spectral range 7500–9000 cm^{-1} . The windows were made of Herasil glass and were coated on both sides by Steeg & Reuter, Giessen, Germany.

This window coating was V type consisting of a thin film of ZrO_2 and a second thin film of MgF_2 . We mention this detail because we observed an interesting phenomenon when working with these windows. When the cryostat was cooled

TABLE I. Measurement parameters for different samples and spectra of solid hydrogen.

Name of spectrum	C ($J=1$) (%)	Crystal temperature (K)	Instrum. FWHM (cm^{-1})	Bandwidth (cm^{-1})	No. of scans	Aperture (mm)
<i>H</i>	1.11 (7)	12.5	0.02	5600 – 10400	400	1.3
<i>I</i>	1.66 (10)	12.5	0.013	5600 – 10400	1100	1.5
<i>J</i>	0.71 (5)	12.5	0.01	5600 – 10400	700	1.5
<i>L</i>	0.09 (1)	12.5	0.007	5600 – 10400	560	1.3
<i>M</i>	0.41 (3)	6.5 – 12.5	0.013	5600 – 10400	1280	1.5
<i>N</i>	<0.1	12.3	0.011	7950 – 8050	840	1.5
<i>O</i>	<0.1	10.8	0.011	7950 – 8050	1200	1.5
<i>P</i>	0.94 (6)	8.5	0.009	8000 – 8100	75	1.5

down to about 12 K we observed a slow decrease, about 3.5% per hour, of transmitted power. We also found a slow increase of the transmission power back to the initial value after about 20 h when the windows were warmed up to room temperature again. This decrease was absent when we used uncoated windows that were simultaneously mounted along the alternate optical axis of our cryostat. The only possible explanation can thus be a slow change of the transmission properties of the coating material when cold. This effect has not been previously observed, and is presumably only obvious because of the high number of passes (32 cold window surfaces). An explanation has not yet been offered.

The procedure of preparing parahydrogen at a desired orthohydrogen impurity level and the growing of a solid hydrogen crystal has been previously described.⁷ The hydrogen cell used in this experiment had an inner diameter of 20 mm and a useful length of 43.5 mm. Having eight passes we thus obtained an absorption path length of 34.8 cm. We used a tungsten light source, a room-temperature $\text{In}_x\text{Ga}_{1-x}\text{As}$ detector, and a CaF_2 beam splitter. The resolution was chosen to fit approximately the width of the observed features; the full resolution of the instrument was not needed. The measurement parameters for each spectrum can be found in Table I.

Spectra were recorded from seven different samples with orthohydrogen content C ranging from 0.09% to 1.66%. Most of the measurements were made at a cell temperature of 12.5 K, one each was made at temperatures of 8.5 and 10.8 K, and one was made at 26 successive points on the temperature scale between 12.5 and 6.5 K. The difficulty with the latter experiment was that we had to find a cooling rate fast enough to perform a sufficient number of scans at a sufficient number of temperature points within the time of the experiment (about 12 h) but not so fast as to destroy the crystal. We found a decrease of 0.6 K/h to be a suitable value, whereas a decrease of 2 K/h caused cracks in the crystal at a temperature below 8.0 K. This behavior can be explained by the time scale of the solid hydrogen self-repair mechanism, which tends to compensate the inevitable stress due to thermal contraction by reordering the crystal structure.¹⁷

The orthohydrogen content was determined from the integrated absorption coefficient of the new $Q_1(1) + Q_1(1)$ double transition, which will be described in Sec. III B.

The original single-beam spectra show unavoidable fringes. We therefore divided the single-beam spectra by

model background functions that simulate the regular fringe patterns. We found that dividing the original spectra by an experimental background spectrum obtained with an empty cell either before or after the experiment did not remove completely the fringing, since due to a slow shift of the fringing pattern throughout the experiment the fringes of the single-beam sample spectra and background spectra did not match.

III. RESULTS

An overview transmittance spectrum of the first overtone region of solid parahydrogen is plotted in Fig. 1. It shows spectrum I of Table I with an orthohydrogen content of 1.66%. The strongest absorption features are indicated by labels. For some of the narrower transitions, such as the $Q_2(0)$, the $Q_1(J) + Q_1(J')$, or the $S_2(0)$, some satellite structure is visible already on this plot. This structure will be treated in detail in the following section. However, the new weak transitions $Y_1(0)$, $Q_1(0) + Q_1(0)$, $U_1(0) + Q_1(1)$, $U_1(0) + S_1(0)$, and $U_1(1) + Q_1(0)$ are not visible at this scale. In Table II we give a comprehensive list of all observed absorption features except the phonon branches in solid parahydrogen at an orthohydrogen content $\leq 1.66\%$ in this region.

A. The $Y_1(0)$ transition

The very weak $Y_1(0)$ transition, the strongest $\Delta J=8$ transition following the $Y_0(0)$,¹ is actually a fundamental rovibrational transition. However, we report it here since it fell in the spectral region of our investigations and we took special efforts to observe it. The extremely high sensitivity necessary to observe this transition was obtained by employing a very narrow bandpass interference filter of 60-cm^{-1} bandwidth and a center wave number of 8000 cm^{-1} . This increased the signal-to-noise ratio by 1.5 orders of magnitude. The scanning time was about 11 h. Figure 2 shows a plot of the absorbance spectrum of the $Y_1(0)$ line for two samples, one with a temperature of 12.3 K (Table I, spectrum *N*) and one with a temperature of 10.8 K (Table I, spectrum *O*). The measurement at 10.8 K was specifically done for confirmation of the initial measurement. The observed linewidth of this transition is dominated by the instrumental resolution, which was 0.011 cm^{-1} for both measurements and was cho-

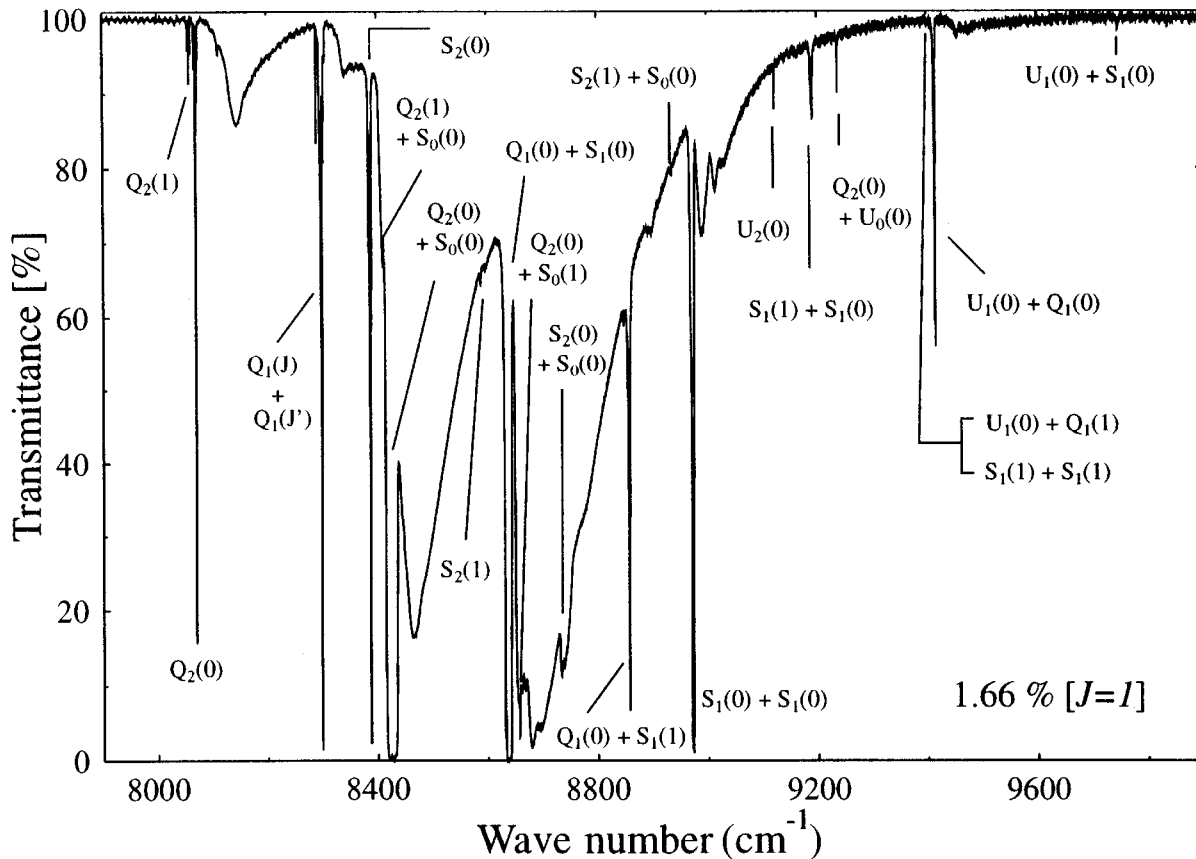


FIG. 1. Overview transmittance spectrum of the first overtone region of solid parahydrogen with a sample path length of 34.8 cm.

sen as a compromise between high resolution and a good signal-to-noise ratio. The integrated absorption coefficient for the $Y_1(0)$ transition was determined to be $2.2(3) \times 10^{-23} \text{ cm}^3/\text{s}$, which is an order of magnitude smaller than that of the $Y_0(0)$ transition, with $2.5(3) \times 10^{-22} \text{ cm}^3/\text{s}$.¹ The identification of this transition as $Y_1(0)$ relies on the line position, the narrowness of the feature, the order of magnitude of its line strength, and the characteristic thermal shift of the line position, which can be clearly seen in Fig. 2. The line position is 7991.861 cm^{-1} at 12.3 K and 7991.801 cm^{-1} at 10.8 K. Assuming that the thermal shift of line positions of solid hydrogen absorptions underlies a law of the form

$$\bar{\nu}(T) = \bar{\nu}(0) + \text{const} \times T^4, \quad (3.1)$$

which is supported by Ref. 18, we can extrapolate the zero-Kelvin line position of the $Y_1(0)$ transition to be 7991.713 cm^{-1} . We will present the thermal shift parameters of several solid hydrogen transitions in Sec. III G of this paper.

Although the prediction of the line position of the $Y_1(0)$ was the first factor in guiding the search and in its identification, we were surprised that this transition shows a quite large deviation from the value predicted by the modified Dunham model introduced by Van Kranendonk and Karl.¹² Until now this model was able to predict all observed transitions of solid hydrogen with an error of less than 3.24 cm^{-1} . However, for the $Y_1(0)$ transition the discrepancy amounts to -5.79 cm^{-1} . In Table III we show the agreement of the modified Dunham model with experimental data

for selected lines. Here the parameters $\mu_1 = 0.03$ and $\mu_2 = -0.005$ from Van Kranendonk's analysis were used for the calculation. To determine these values Van Kranendonk employed six selected transitions from the fundamental and first overtone band of solid parahydrogen. In Sec. IV A we present a calculation where we have refitted the parameters μ_1 and μ_2 using the experimentally observed values of all the 15 transitions in Table III.

B. The $Q_1(1) + Q_1(1)$ transition

The $Q_1(1) + Q_1(1)$ transition was reported in Ref. 14 for normal hydrogen, although only a single broad feature was seen that included all three $Q_1(J) + Q_1(J')$ transitions ($J, J' = 0, 1$). It was observed in highly enriched parahydrogen for the first time by Steinhoff.¹⁹ Figure 3 shows an absorbance spectrum of the whole $Q_1(J) + Q_1(J')$ region for two different orthohydrogen impurity levels (Table I, spectra J and L). The $Q_1(1) + Q_1(1)$ transition is interesting because it is a double transition in an orthohydrogen pair and therefore consists entirely of fine structure. The orthohydrogen pair interaction is dominated by the electric quadrupole-quadrupole (EQQ) interaction and has been studied in detail in several previous works.^{7,8,20-22} The orthohydrogen pair fine structure observed in the ground-state microwave spectrum²⁰ and with the $Q_1(1)$ transition,²² in particular, have been extensively studied. There are only three clearly visible absorption peaks of the $Q_1(1) + Q_1(1)$ transition, which are marked with α , β , and γ in Fig. 3. There are some weak features between β and γ that can also be interpreted

TABLE II. Line positions and integrated absorption coefficients of infrared transitions in the first overtone region of solid parahydrogen with orthohydrogen impurity levels $\leq 1.66\%$.

Transition	Line position (cm^{-1})	$\tilde{\alpha}^a$ ($\text{cm}^3 \text{s}^{-1}$)	Previously observed
$Y_1(0)$	7991.71 ^b	$2.2(3) \times 10^{-23}$	(This work)
$Q_2(1)$	8058.72 ^b	$1.3(1) \times 10^{-17}$	Refs. 19,14, ^c 15
$Q_2(0) + Q_0(1)$	8070.44 ^b	$3.8(1) \times 10^{-16}$	Refs. 8,14,15
$Q_1(1) + Q_1(1)$	8293.00 ^b	$1.9(4) \times 10^{-16}$	Ref. 19
$Q_1(1) + Q_1(0)$	8299.6 ^d	$1.2(2) \times 10^{-15}$	Refs. 14,15
$Q_1(0) + Q_1(0)$	8306.0 ^d	$1.8(4) \times 10^{-19}$	This work
$S_2(0)$	8387.34 ^b	$1.2(2) \times 10^{-17}$	Refs. 14,15
$Q_2(1) + S_0(0)$	8402 – 8414 ^e	$1.9(2) \times 10^{-16}$	Ref. 14 ^c
$Q_2(0) + S_0(0)$	8414 – 8435 ^e	... ^f	Refs. 14 ^c , 15
$S_2(1)$	8588.20	$2.0(3) \times 10^{-17}$	Ref. 14 ^c
$Q_1(0) + S_1(0)$,			
$Q_1(1) + S_1(0)$	8631 – 8643 ^e	... ^f	Refs. 14,15
$Q_2(0) + S_0(1)$	8657.29	$2.5(3) \times 10^{-16}$	Ref. 14 ^c
$S_2(0) + S_0(0)$	8731 – 8753 ^e	$2.9(4) \times 10^{-17}$	Ref. 19
$Q_1(0) + S_1(1)$	8857.3 ^d	$1.1(2) \times 10^{-15}$	Refs. 14,15
$S_2(1) + S_0(0)$	8931 – 8951 ^e	$5.8(8) \times 10^{-17}$	Ref. 14 ^c
$S_1(0) + S_1(0)$	8971 – 8974 ^e	$3.8(2) \times 10^{-17}$	Refs. 14,15
$U_2(0)$	9122.21 ^b	$1.1(1) \times 10^{-19}$	Ref. 15
$S_1(1) + S_1(0)$	9189 – 9192 ^e	$9.5(8) \times 10^{-17}$	Ref. 14 ^c
$Q_2(0) + U_0(0)$	9237.35 ^b	$1.4(4) \times 10^{-19}$	Ref. 15
$U_1(0) + Q_1(1)$	9406.6 – 9409.7 ^g	$2.4(4) \times 10^{-18}$	This work
$U_1(0) + Q_1(0)$	9414.15 ^d	$2.8(3) \times 10^{-18}$	Ref. 15
$U_1(0) + S_1(0)$	9745 – 9751 ^e	$1.1(2) \times 10^{-19}$	This work
$U_1(1) + Q_1(0)$	9837.4 ^d	$2.2(3) \times 10^{-18}$	This work

^aIntegrated absorption coefficient per molecule per unit volume.

^bLine position extrapolated to a crystal temperature of 0 K. Others are for 12.5 K.

^cObserved previously only in normal hydrogen.

^dBroadened by vibron hopping.

^eBroadened by roton hopping.

^fToo strong to be determined.

^gSplit by orthohydrogen pair interaction.

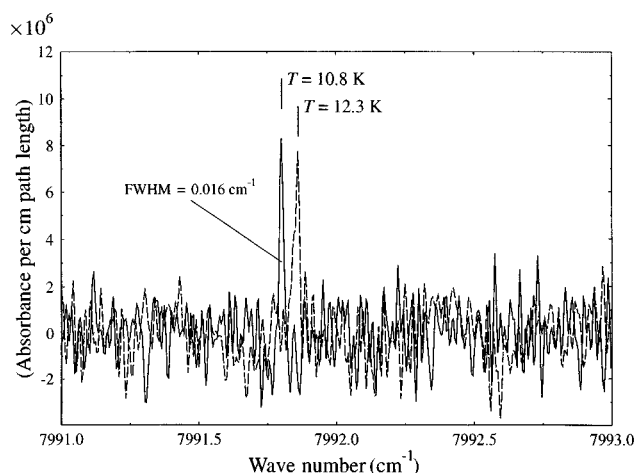


FIG. 2. Absorbance spectra of the $Y_1(0)$ transition in solid hydrogen at two different crystal temperatures.

TABLE III. Rovibrational transitions of solid hydrogen reproduced with a modified Dunham model: predictions.

Transition	ν_{obs} (cm^{-1})	ν_{calc}^a (cm^{-1})	$\nu_{\text{obs}} - \nu_{\text{calc}}$ (cm^{-1})
$U_0(0)$	1167.12	1166.79	0.33
$W_0(0)$	2410.54	2410.81	-0.27
$W_0(1)$	3063.48	3064.05	-0.57
$Y_0(0)$	4044.18	4046.19	-2.01
$Q_1(1)$	4146.51	4147.24	-0.73
$S_1(1)$	4704.44	4704.21	0.23
$U_1(0)$	5261.28	5261.99	-0.71
$U_1(1)$	5684.61	5685.69	-1.08
$W_1(0)$	6441.81	6443.96	-2.15
$W_1(1)$	7055.37	7058.61	-3.24
$Y_1(0)$	7991.71	7997.50	-5.79
$Q_2(1)$	8058.72	8059.80	-1.08
$Q_2(0)$	8070.44	8071.18	-0.74
$U_2(0)$	9122.21	9125.42	-3.21
$Q_3(0)$	11758.73	11759.43	-0.70

^aCalculated from the modified Dunham model, Van Kranendonk and Karl (Ref. 12), with $\mu_1 = 0.03$, $\mu_2 = -0.005$.

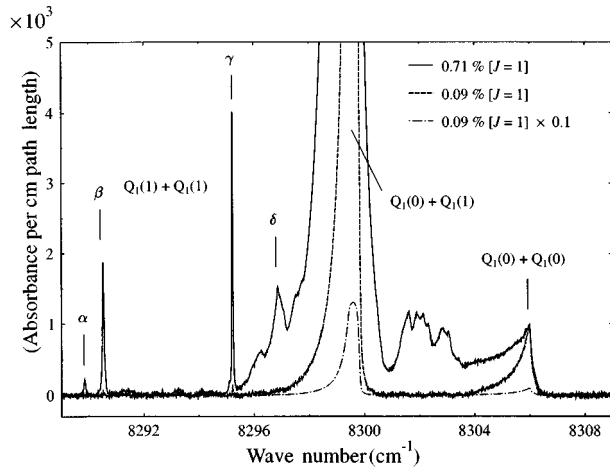


FIG. 3. Spectrum of the $Q_1(J) + Q_1(J')$ region in solid hydrogen for two different orthohydrogen impurity levels.

as components of the $Q_1(1) + Q_1(1)$ pair transition. However, we will concentrate now on the three strong ones. Our interpretation of these features is illustrated in Fig. 4, which shows a diagram of the orientational energy levels of the orthohydrogen pair in the ground state as well as in the state where both molecules of the pair are vibrationally excited ($v_a = v_b = 1$). For this excited state we expect a similar splitting pattern as for the $Q_2(1)$ transition (see Sec. III E) since it should not make too great a difference for the EQQ coupling constant whether one molecule of the orthohydrogen pair is doubly excited or both molecules are singly excited. We attribute the two strongest absorptions β and γ to the fine structure transitions between the $|2,1\rangle_{\pm}$ and $|1,1\rangle_{\pm}$ orientational states. This is supported by two facts. First, the transitions $|2,1\rangle_{\pm} \rightleftharpoons |1,1\rangle_{\pm}$ are by far the strongest ones in the pair spectra of the $Q_1(1)$ and $Q_2(1)$ transitions. Second, the ratio of the intensities of line β and line γ should be the ratio of the Boltzmann factors in their ground states, since the dipole matrix elements for these transitions are invariant under permutation of the initial and final orientational state. According to our assignment, the term value difference be-

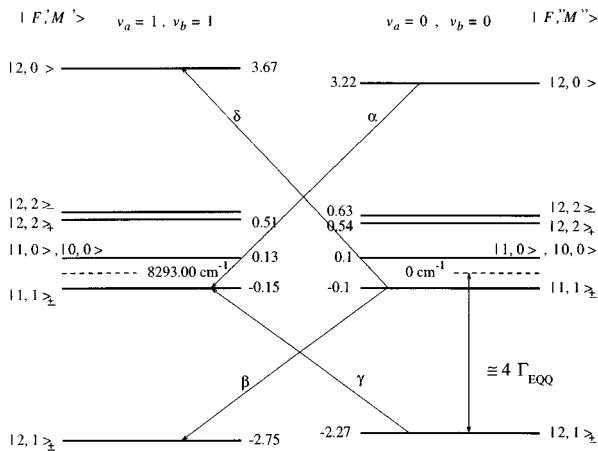


FIG. 4. Term diagram for the $Q_1(1) + Q_1(1)$ transition in solid hydrogen. On the right is the term diagram of a nearest-neighbor orthohydrogen pair in the vibrational ground state, the left diagram is for the excited state. Numerical values are in cm^{-1} .

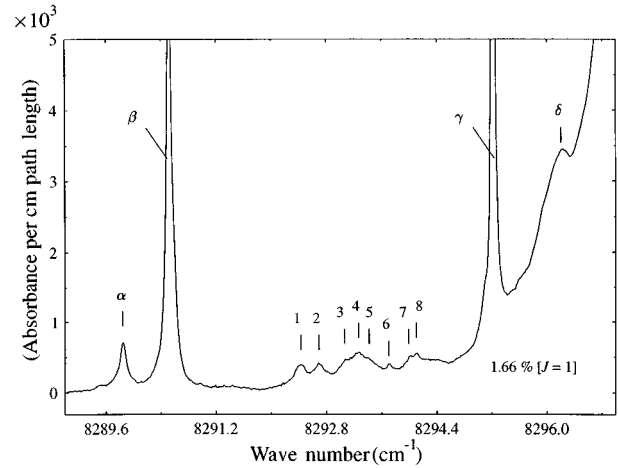


FIG. 5. Fine structure of the $Q_1(1) + Q_1(1)$ transition of solid hydrogen at an orthohydrogen content of 1.66%. The assignment is given in Table IV.

tween the lower levels of the β and the γ lines amounts to about 2.2 cm^{-1} . We have analyzed spectra of two different crystals, one at 12.5 K and one at 6.5 K. The Boltzmann relation for the ratio of the populations in the lower states of the two transitions

$$\frac{N(\gamma)}{N(\beta)} = e^{hc(2.2\text{cm}^{-1}/kT)} \quad (3.2)$$

gives the value 1.29 for $T=12.5 \text{ K}$ and 1.63 for $T=6.5 \text{ K}$. The experimental ratios of the integrated absorption coefficients $\alpha(\gamma)/\alpha(\beta)$ were determined to be 1.3 for $T=12.5 \text{ K}$ and 1.7 for 6.5 K, which is in fine agreement with this assignment.

According to the line position the α peak can be either the transition $|2,1\rangle_{\pm} \leftarrow |2,2\rangle_{\pm}$ or $|1,1\rangle_{\pm} \leftarrow |2,0\rangle$. We can exclude the first one for the following reason: if this transition were $|2,1\rangle_{\pm} \leftarrow |2,2\rangle_{\pm}$ we must find the equivalent transition $|2,2\rangle_{\pm} \leftarrow |2,1\rangle_{\pm}$, which would lie at 8295.95 cm^{-1} near the γ line and should be even stronger than the α line because of the lower ground-state energy. However, we find no appropriate absorption peak at this position. The $|2,0\rangle \leftarrow |1,1\rangle_{\pm}$ transition, however, would be at 8296.8 cm^{-1} and there is a strong feature with a sharp peak labeled with δ that appears to be superimposed on a broad satellite feature of the neighboring $Q_1(0) + Q_1(1)$ double transition; it is even sharper at lower temperature and lower orthohydrogen impurity levels. In Fig. 5 we show another spectrum of the $Q_1(1) + Q_1(1)$ transition taken at an orthohydrogen impurity level of 1.66% (spectrum I of Table I). We find here some additional weak absorption features labeled with numbers 1 to 8. Table IV gives an assignment of all fine structure peaks that we could attribute to the $Q_1(1) + Q_1(1)$ transition. The extreme dominance of the β and γ fine structure components indicates that the transition dipole moment cannot be calculated by the same procedure as for the satellite structure of the $Q_1(1)$ and $Q_2(1)$ transitions (see Sec. III E) although in those cases these are also the strongest components.

The splitting pattern of the ground state has been adopted from Ref. 20. We give numerical term values in the

TABLE IV. Orthohydrogen pair fine structure in the region of the $Q_1(1) + Q_1(1)$ transition.

Label ^a	$\bar{\nu}$ (cm^{-1})	$\Delta\bar{\nu}^b$ (cm^{-1})	Assignment $ F', M'\rangle \leftarrow F'', M''\rangle$
α	8289.62	-3.38	$ 1,1\rangle_{\pm} \leftarrow 2,0\rangle$
β	8290.35	-2.65	$ 2,1\rangle_{\pm} \leftarrow 1,1\rangle_{\pm}$
γ	8295.12	2.12	$ 1,1\rangle_{\pm} \leftarrow 2,1\rangle_{\pm}$
δ	8296.77	3.77	$ 2,0\rangle \leftarrow 1,1\rangle_{\pm}$
1	8292.34	-0.66	$ 1,1\rangle_{\pm} \leftarrow 2,2\rangle_{+}$
2	8292.58	-0.42	$ 1,0\rangle, 0,0\rangle \leftarrow 2,2\rangle_{+}$
3	8292.97	-0.03	. . . ^c
4	8293.17	0.17	. . . ^c
5	8293.30	0.30	. . . ^c
6	8293.61	0.61	$ 2,2\rangle_{+} \leftarrow 1,1\rangle_{\pm}$
7	8293.92	0.92	. . . ^c
8	8294.01	1.01	. . . ^c

^aSee Fig. 5.

^b $\Delta\bar{\nu}$ is the relative position referred to 8293.00 cm^{-1} .

^cThese absorptions are attributed to the satellite structure of the $Q_1(0) + Q_1(1)$ transition.

excited state only for those levels that were determined by our assignment. The hypothetical zero-interaction line position for the $Q_1(1) + Q_1(1)$ transition is then $8293.00(5) \text{ cm}^{-1}$. By zero interaction we mean the absence of any anisotropic forces between the molecules. For twice the line position of the $Q_1(1)$ single transition we find a value of $8293.104(2) \text{ cm}^{-1}$. These two values may differ, because in the case of the $Q_1(1) + Q_1(1)$ double transition the local symmetry around an orthohydrogen molecule is perturbed by the other orthohydrogen molecule. We learn from these data that this isotropic interaction must be on the order of 0.1 cm^{-1} .

Since the line strength of the $Q_1(1) + Q_1(1)$ transition is in first order proportional to the square of the orthohydrogen impurity level, these lines may serve as ideal probes of the orthohydrogen content in the range 0 – 2 %. We used some of the spectra measured by Steinhoff,¹⁹ for which the orthohydrogen content was determined directly from the $Q_1(1)$ transition, to determine the sum of the integrated absorption coefficients of the β and γ components and obtained a value of $1.9 \pm 0.4 \times 10^{-16} \text{ cm}^3/\text{s}$. We then used this value to determine the orthohydrogen contents of our samples.

C. The $Q_1(0) + Q_1(0)$ transition

Probably the most surprising feature of this work can be seen on the right side of the spectrum in Fig. 3, located at 8306 cm^{-1} . According to the line position, the only interpretation of this peak is that it is the double transition $Q_1(0) + Q_1(0)$. The integrated absorption coefficient per molecule, $\bar{\alpha}$, is $1.8(4) \times 10^{-19} \text{ cm}^3/\text{s}$. The line shape of this absorption feature comes out most clearly at an orthohydrogen impurity level of 0.09%. Another support of this interpretation is the unsymmetric line shape with a sharp cutoff at the high-wave-number side, which is present in all double transitions involving a $Q_1(0)$. However, in previous works it has been underlined that this double transition is strictly forbidden in the infrared, because neither of the involved

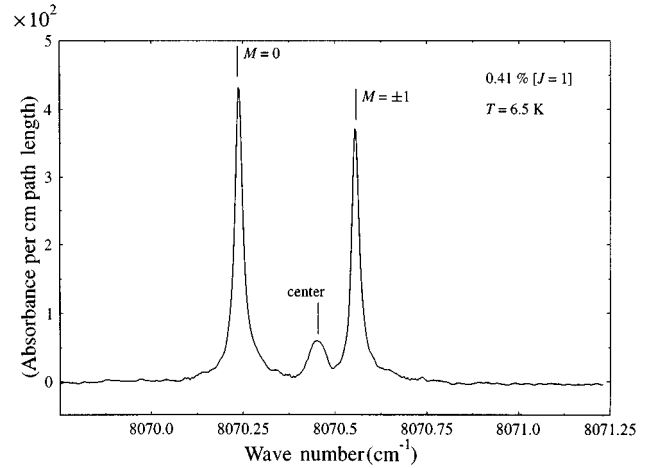


FIG. 6. Spectrum of the $Q_2(0)$ transition in nearly pure solid parahydrogen.

parahydrogen molecules can change any projection of its angular momentum. Our assumption when we saw this transition for the first time was that this might be actually a triple transition with one assisting orthohydrogen neighbor. However, from further measurements with orthohydrogen impurity levels ranging from 0.09% to 1.66% we learned that this transition is independent of the orthohydrogen content and thus no orthohydrogen molecule can be involved. In Fig. 3 the invariance of the peak height of the $Q_1(0) + Q_1(0)$ transition for two different orthohydrogen impurity levels can be easily verified. The mechanism of this transition is planned to be the subject of a separate publication.

D. The $Q_2(0)$ transition

1. Crystal field splitting

It was already found by Oka and co-workers⁸ that this line is split into two components with an interval of about 0.34 cm^{-1} due to the crystal field perturbation of the nearest-neighbor orthohydrogen molecule that induces this transition. The low-frequency component corresponds to transitions of the orthohydrogen molecule into the $M=0$ substate and the high-frequency component corresponds to transitions into the degenerate $M=\pm 1$ substates. In Fig. 6 we show a spectrum of this transition (spectrum M of Table I), which was taken at an orthohydrogen impurity level of 0.41% and a temperature of 6.5 K. It is necessary to have both of these parameters this low or lower in order to resolve fully a third peak between the two strong components. According to the theory outlined in Ref. 23 this peak can clearly be interpreted as the $Q_2(0)$ transition of a next-nearest-neighbor ortho-parahydrogen pair. It has a lower intensity and a smaller scale of the splitting because the separation of a next-nearest-neighbor pair is a factor of $\sqrt{2}$ larger than that of the nearest-neighbor pair, resulting in much weaker effects of intermolecular forces. This absorption feature can thus be seen as a condensed image of the two larger peaks, but they cannot be resolved. The full width at half maximum (FWHM) of the two strong transitions is 0.029 cm^{-1} , which should mainly be due to the $\nu=2$ vibron hopping and experimental broadening mechanisms such as temperature variation over the sample. The FWHM of the central peak is 0.052 cm^{-1} ,

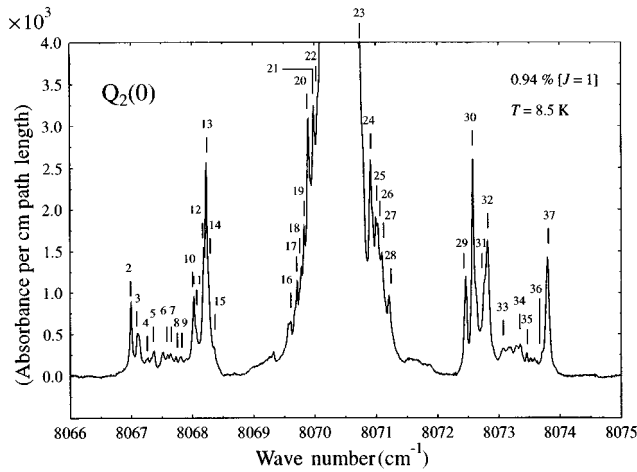


FIG. 7. Satellite structure of the $Q_2(0)$ transition in solid hydrogen at an orthohydrogen content of 0.94%. For assignment of satellite transitions see Table V.

which indicates that it consists indeed of more than one component. The center label in Fig. 6 indicates the origin of the $Q_2(0)$ transition, i.e., the position where this absorption peak would lie in the hypothetical case without crystal field splitting. It is obtained from the positions of the two strong peaks using the theoretical expression for the crystal field splitting¹³ in terms of the crystal field splitting parameter ϵ_{2c} ,

$$\tilde{\nu}(M=0) = \frac{2}{5} \epsilon_{2c}, \quad (3.3)$$

$$\tilde{\nu}(M=\pm 1) = -\frac{1}{5} \epsilon_{2c}. \quad (3.4)$$

The parameter ϵ_{2c} for the $v=2$ excited state can hence be determined for a crystal temperature of 6.5 K to be $-0.528(2) \text{ cm}^{-1}$. In Sec. IV D we present an analysis of the variation of this value as a function of temperature and extrapolate it to the zero-Kelvin point.

2. Satellite structure

At various orthohydrogen impurity levels we were able to observe satellite peaks of the $Q_2(0)$ transition due to the orthohydrogen pair interaction. Employing the narrow band-pass filter mentioned in Sec. III A, tilted a little bit to shift the center wave number from 8000 to 8065 cm^{-1} , and lowering the crystal temperature to 8.5 K, we recorded the spectrum of the $Q_2(0)$ transition, which is plotted in Fig. 7 (Table I, spectrum P). The absorbance scale is enhanced, so that the three peaks in Fig. 6 described in the previous paragraph are off scale. We find more than 30 weak satellite peaks around this transition, with linewidths of $0.03\text{--}0.06 \text{ cm}^{-1}$. Table V gives a list of all peaks in this region, which we have assigned and which are labeled in Fig. 7. The two weak outermost components, numbered 1 and 38, are outside the wave-number limits of Fig. 7. We have distinguished three different classes of line strength: class A means strong, class B means weaker but undoubtedly present, and class C lines have a line strength barely above the noise level or are shoulders of stronger peaks. We assume that the assignment of these satellite peaks to the appropriate orthohydrogen pair fine structure transitions can be made analogously to the as-

signment of those of the $Q_1(0)$ transition in Sec. 4.5 of Ref. 7. However, many more peaks can be identified in the $Q_2(0)$ satellite spectrum, since the central line and the satellite lines are a factor of 10 narrower than the lines found for the fundamental transition. In a first approach we assumed the splitting pattern of the orientational states in the vibrationally excited state to be exactly the same as in the ground state, which is known precisely from microwave experiments.²⁰ The validity of this approximation is given by the fact that the orthohydrogen pair spectrum of each $Q_v(0)$ type of transition is induced by a pair of orthohydrogen molecules in the direct neighborhood of the vibrationally excited parahydrogen molecule while the orthohydrogen molecules themselves remain in the vibrational ground state. We assigned the line positions given in Table V to transitions between these energy levels, which led to a weighted standard deviation of 0.063 cm^{-1} . We then refined the term values in the excited state by doing a linear least-squares fit that resulted in the diagram of Fig. 8 and a standard deviation of 0.0311 cm^{-1} . This is larger than that found for the assignment of the $Q_2(1)$ pair structure (see Sec. III E). We attribute the mismatch to the fact that there is a crystal field contribution to the excited state levels of the orthohydrogen pair, too, which can be of the order of up to 0.1 cm^{-1} according to our calculations. However, a detailed analysis of this effect is not possible with our data since there are several different geometries of the three molecules involved, an orthohydrogen pair and a parahydrogen molecule, which leads to a manifold of many closely spaced energy levels.

E. The $Q_2(1)$ transition

Simultaneously with the $Q_2(0)$ transition we recorded the $Q_2(1)$ transition, which also shows satellite peaks, as can be seen in Fig. 9. These absorptions have FWHM linewidths of $0.025\text{--}0.04 \text{ cm}^{-1}$ and are thus narrower than those for the $Q_2(0)$ transition. The linewidth of the $Q_2(1)$ main peak is 0.041 cm^{-1} with an orthohydrogen content of 0.94% and 0.031 cm^{-1} in nearly pure parahydrogen (0.09% $J=1$). Since there should be no broadening due to vibron hopping and no crystal field splitting, we expected a much narrower line. The $Q_1(1)$ transition, with an observed (instrumentally limited) FWHM linewidth of 0.016 cm^{-1} ,⁷ is actually much narrower than the $Q_2(1)$. We do not have an explanation for this observation at the moment.

For the orthohydrogen pair fine structure we worked out an assignment which is given in Table VI. The corresponding term diagram is shown in Fig. 10. The vibrational excitation is localized on one of the two orthohydrogen molecules, as is indicated in Fig. 10 by $v_a=2, v_b=0$. We did not have to consider different subsystems due to symmetric and antisymmetric excited states as in the case of the $Q_1(1)$ pair structure, because from Ref. 23 we can deduce that the corresponding splitting should be only about 0.005 cm^{-1} , which is much less than the observed linewidths. The weighted standard deviation of our assignment is 0.0147 cm^{-1} , which is better than for the $Q_2(0)$ transition. The splitting pattern in the excited state looks much different from that in the ground state because now one of the orthohydrogen pair molecules is doubly vibrationally excited, which

TABLE V. Orthohydrogen pair fine structure of the $Q_2(0)$ transition.

Label ^a	Class	$\tilde{\nu}$ (cm^{-1})	$\Delta\tilde{\nu}^b$ (cm^{-1})	Assignment $ F', M'\rangle \leftarrow F'', M''\rangle$	$\Delta\tilde{\nu}_{\text{Ass.}}^c$ (cm^{-1})
1	C	8064.941	-5.523	$ 2,1\rangle_+ \leftarrow 2,0\rangle$	-5.486
2	B	8066.995	-3.469	$ 1,1\rangle_+ \leftarrow 2,0\rangle$	-3.437
3	B	8067.099	-3.365	$ 1,1\rangle_- \leftarrow 2,0\rangle$	-3.326
4	C	8067.269	-3.195	$ 1,0\rangle \leftarrow 2,0\rangle$	-3.257
5	B	8067.372	-3.092	$ 0,0\rangle \leftarrow 2,0\rangle$	-3.063
6	C	8067.597	-2.867	$ 2,1\rangle_+ \leftarrow 2,2\rangle_-$	-2.898
7	C	8067.645	-2.819	$ 2,1\rangle_+ \leftarrow 2,2\rangle_+$	-2.807
8	C	8067.733	-2.731	$ 2,2\rangle_+ \leftarrow 2,0\rangle$	-2.664
9	C	8067.811	-2.653	$ 2,2\rangle_- \leftarrow 2,0\rangle$	-2.567
10	B	8068.030	-2.434	$ 2,1\rangle_- \leftarrow 1,0\rangle$	-2.426
11	C	8068.063	-2.401	$ 2,1\rangle_+ \leftarrow 0,0\rangle$	-2.383
12	B	8068.194	-2.270	$ 2,1\rangle_- \leftarrow 1,1\rangle_-$	-2.263
13	A	8068.237	-2.228	$ 2,1\rangle_- \leftarrow 1,1\rangle_+$	-2.235
14	C	8068.270	-2.194	$ 2,1\rangle_+ \leftarrow 1,1\rangle_-$	-2.184
15	C	8068.355	-2.109	$ 2,1\rangle_+ \leftarrow 1,1\rangle_+$	-2.156
16	B	8069.606	-0.858	$ 1,1\rangle_+ \leftarrow 2,2\rangle_-$	-0.849
17	B	8069.716	-0.749	$ 1,1\rangle_+ \leftarrow 2,2\rangle_+$	-0.758
18	C	8069.752	-0.712	$ 1,1\rangle_- \leftarrow 2,2\rangle_-$	-0.738
19	B	8069.831	-0.633	$ 1,1\rangle_- \leftarrow 2,2\rangle_+$	-0.647
20	B	8069.897	-0.567	$ 1,0\rangle \leftarrow 2,2\rangle_-$	-0.569
21	B	8069.988	-0.476	$ 1,0\rangle \leftarrow 2,2\rangle_+$	-0.478
22	C	8070.009	-0.455	$ 0,0\rangle \leftarrow 2,2\rangle_-$	-0.475
23	B	8070.749	0.285	$ 0,0\rangle \leftarrow 1,1\rangle_+$	0.267
24	B	8070.915	0.451	$ 2,2\rangle_+ \leftarrow 0,0\rangle$	0.438
25	B	8071.000	0.536	$ 2,2\rangle_- \leftarrow 0,0\rangle$	0.535
26	B	8071.034	0.570	$ 2,2\rangle_- \leftarrow 1,0\rangle$	0.572
27	B	8071.094	0.630	$ 2,2\rangle_+ \leftarrow 1,1\rangle_-$	0.638
28	B	8071.210	0.746	$ 2,2\rangle_- \leftarrow 1,1\rangle_-$	0.738
29	A	8072.459	1.995	$ 1,1\rangle_+ \leftarrow 2,1\rangle_+$	2.036
30	A	8072.579	2.115	$ 1,1\rangle_+ \leftarrow 2,1\rangle_-$	2.058
31	B	8072.623	2.159	$ 1,1\rangle_- \leftarrow 2,1\rangle_-$	2.147
32	B	8072.818	2.353	$ 1,0\rangle \leftarrow 2,1\rangle_-$	2.338
33	C	8073.071	2.607	$ 2,0\rangle \leftarrow 2,2\rangle_-$	2.600
34	C	8073.351	2.886	$ 2,2\rangle_+ \leftarrow 2,1\rangle_-$	2.831
35	C	8073.457	2.993	$ 2,2\rangle_- \leftarrow 2,1\rangle_-$	2.928
36	C	8073.581	3.117	$ 2,0\rangle \leftarrow 0,0\rangle$	3.114
37	A	8073.798	3.334	$ 2,0\rangle \leftarrow 1,1\rangle_+$	3.342
38	B	8075.959	5.495	$ 2,0\rangle \leftarrow 2,1\rangle_+$	5.485

^aSee Fig. 7.

^b $\Delta\tilde{\nu}$ is the relative position referred to 8070.464 cm^{-1} , which is the origin of the $Q_2(0)$ transition.

^cTerm value differences obtained from this assignment. See also Fig. 8.

leads to a higher expectation value of its quadrupole moment and thus to a larger quadrupole coupling constant Γ_{EQQ} . We used the term values of the excited state obtained from our assignment to determine semiphenomenological force constants established in the theory of Harris.²¹ In a nonlinear fit we obtained the following values for the three most important of these constants for the doubly vibrationally excited state: $\tilde{\Gamma} = 0.668 \text{ cm}^{-1}$, $\tilde{\epsilon}_2 = -0.0164 \text{ cm}^{-1}$, and $\tilde{\epsilon}_0 = 0.0202 \text{ cm}^{-1}$. We should note that we were not able to distinguish between in-plane and out-of-plane pair configurations. All other constants did not significantly deviate from their values in the vibrational ground state.

This assignment is essentially based on the line positions. We can verify its correctness by comparing the experimental line strengths with the calculated values of the dipole moment transition moments. This calculation was first performed by Chan²² and later, with some corrections, by Byers²⁴ for the orthohydrogen pair structure of the $Q_1(1)$ transition. Because of the similarity of the $Q_1(1)$ and $Q_2(1)$ transitions as far as the orientational states are concerned we use the values of the $Q_1(1)$ transition moments for comparison in Table VI. We find a satisfactory agreement in most cases. However, there are some transitions that are about an order of magnitude stronger or weaker than predicted and

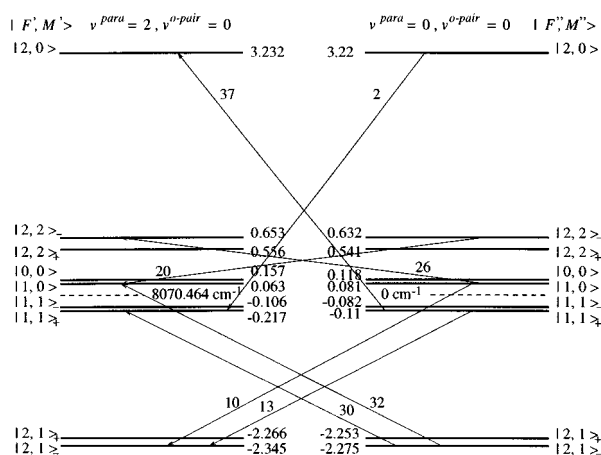


FIG. 8. Term diagram and the strongest orthohydrogen pair transitions associated with the $Q_2(0)$ transition. Transition labels are identical with those of Fig. 7 Numerical values are in cm^{-1} .

even one (transition 16) that should be forbidden according to the theory. For the very weak lines the determination of the observed intensity by a simple numerical integration method cannot be expected to be more accurate than half an order of magnitude.

The domains of the pair fine structure transitions of the $Q_2(0)$ and $Q_2(1)$ do not overlap as they do in the case of the $Q_1(J)$.⁷ In our assignment the highest component (28) of the $Q_2(1)$ structure is at 8064.667 cm^{-1} , marking the end of this domain whereas the lowest component (1) of the $Q_2(0)$ structure starts at 8064.941 cm^{-1} .

F. New double transitions

In the wave-number region $9400\text{--}9900 \text{ cm}^{-1}$ we have observed three features that we interpret to be new double transitions. These are the transitions $U_1(0) + Q_1(1)$ at $9407.67(5) \text{ cm}^{-1}$, $U_1(0) + S_1(0)$ at $9745.3 - 9750.1 \text{ cm}^{-1}$, and $U_1(1) + Q_1(0)$ at 9837.34 cm^{-1} . The last two could be assigned without hesitation according to their line positions. The structure of the $U_1(0) + S_1(0)$ transition ex-

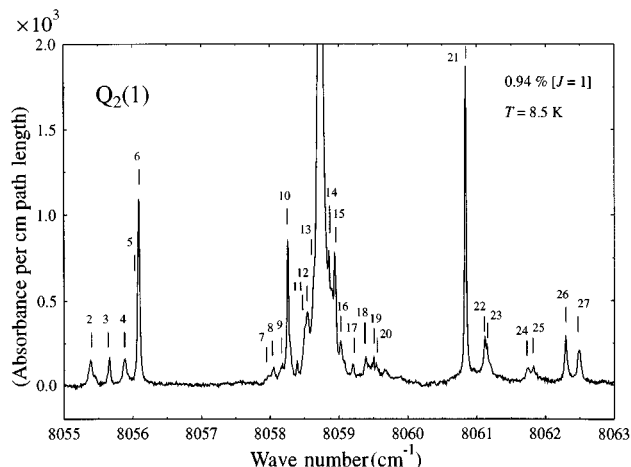


FIG. 9. Satellite structure of the $Q_2(1)$ transition in solid hydrogen at an orthohydrogen content of 0.94%. For assignment of satellite transitions see Table VI.

tends over about 5 cm^{-1} due to the $J=2$ roton hopping mechanism. The $U_1(1)+Q_1(0)$ is a single feature with a lineshape analogous to that of $Q_1(0)$. For the $U_1(0)+Q_1(1)$ we find three absorption peaks at the positions 9406.58 cm^{-1} , 9407.67 cm^{-1} , and 9409.66 cm^{-1} . These peaks could only be seen in spectrum I of Table I, taken with the highest $J=1$ content and with the highest number of scans. From the sum of the line positions of single transitions we can predict a value of 9408.04 cm^{-1} for the $U_1(0)+Q_1(1)$ double transition, indicated in Fig. 11. As in the case of $Q_1(1)+Q_1(1)$ we find only fine structure for this transition. The three peaks shown in Fig. 11 correspond to the strongest components in the fine structure associated with the $U_1(0)$ transition, reported previously.⁷ In addition, they are nearly identical to the structure we have identified as the $U_0(0)+Q_1(1)$ double transition at 5314 cm^{-1} which will be reported in a later publication.

The new double transitions together with their integrated absorption coefficients per molecule per unit volume are included in Table II.

G. Measurements of thermal shifts

As mentioned in Sec. II we were able to scan the whole overtone spectrum at 26 different temperature points starting at 12.5 K and extending down to 6.5 K (Table I, spectra *M*). The most striking observation is that all absorption lines are redshifted by up to 0.2 cm^{-1} upon cooling over this range. Such a shift was previously reported for the $Q_1(1)$ transition in Ref. 18. The temperature change also affects the linewidths — they are narrower when the crystal is colder — and all spectral parameters that depend on the intermolecular separation R such as the electric quadrupole-quadrupole coupling constant Γ_{EQQ} . The line intensities should also become larger at lower temperature due to the R dependence of the infrared induction mechanisms, but we were not able to detect significant intensity differences. All these effects are largely due to the thermal contraction of the hydrogen crystal. In Fig. 12 an example of thermal effects in the spectrum of the $Q_2(0)$ transition is shown. By lowering the crystal temperature from 12.5 to 6.5 K the FWHM of the two strong components is reduced by a factor of 2 and the positions shift by about 0.12 cm^{-1} to the red. However, the shifts are not equal since the parameter that determines the splitting — the crystal field constant ϵ_{2c} — is a function of R , too. A discussion of the temperature variation of ϵ_{2c} will be given in Sec. IV D. We have obtained highly precise values for the positions of line centers by using the FITMAS program of Schreier (DLR, Germany).²⁵ In a procedure similar to that of INTBAT,²⁶ this program fits model function line shapes to the observed spectral data, however, with some extended options. The quality of the determination of the line positions can be judged by the small scatter of the data points in Fig. 13 where we have plotted the line position of the $Q_2(1)$ transition and a fitted empirical function versus the temperature.

We have also determined the temperature dependence of the quadrupole-quadrupole coupling constant Γ_{EQQ} in the temperature region mentioned above. As can be seen in the term diagram of Fig. 4 the separation $\Delta\tilde{\nu} = \tilde{\nu}_\gamma - \tilde{\nu}_\beta$ between the β and the γ components of the $Q_1(1) + Q_1(1)$ transi-

TABLE VI. Orthohydrogen pair fine structure of the $Q_2(1)$ transition.

Label ^a	Class	$\tilde{\nu}$ (cm^{-1})	$\Delta\tilde{\nu}^b$ (cm^{-1})	Assignment $ F', M'\rangle \leftarrow F'', M''\rangle$	$\Delta\tilde{\nu}_{\text{Ass.}}^c$ (cm^{-1})	Obs. rel. ^d intensity	Calc. rel. ^d intensity ^e
1	C	8052.779	-5.960	$ 2,1\rangle_{\pm} \leftarrow 2,0\rangle$	-5.968	0.009	0.007
2	B	8055.384	-3.356	$ 1,1\rangle_{-} \leftarrow 2,0\rangle$	-3.351	0.238	0.135
3	B	8055.660	-3.079	$ 0,0\rangle \leftarrow 2,0\rangle$	-3.065	0.090	0.135
4	B	8055.882	-2.857	$ 2,1\rangle_{\pm} \leftarrow 0,0\rangle$	-2.866	0.143	0.206
5	C	8056.070	-2.670	$ 2,1\rangle_{\pm} \leftarrow 1,1\rangle_{-}$	-2.663	. . . ^f	
6	A	8056.092	-2.647	$ 2,1\rangle_{\pm} \leftarrow 1,1\rangle_{+}$	-2.635	0.762	0.680 ^g
7	C	8057.971	-0.768	$ 1,1\rangle_{-} \leftarrow 2,2\rangle_{-}$	-0.763	. . . ^f	0.028
8	B	8058.052	-0.688	$ 1,1\rangle_{-} \leftarrow 2,2\rangle_{+}$	-0.672	0.062	0.035
9	C	8058.179	-0.560	$ 1,0\rangle \leftarrow 2,2\rangle_{-}$	-0.557	0.006	0.062
10	A	8058.260	-0.479	$ 2,1\rangle_{\pm} \leftarrow 2,1\rangle_{\pm}$	-0.492	0.429	0.132
11	B	8058.395	-0.344	$ 0,0\rangle \leftarrow 2,2\rangle_{+}$	-0.386	0.029	0.041
12	B	8058.544	-0.195	$ 1,1\rangle_{-} \leftarrow 1,0\rangle$	-0.212	0.176	0.058
13	B	8058.645	-0.094	$ 1,1\rangle_{+} \leftarrow 1,1\rangle_{-}$	-0.094	. . . ^f	0.013
14	B	8058.855	0.116	$ 1,0\rangle \leftarrow 1,1\rangle_{-}$	0.157	0.041	0.058
15	B	8058.938	0.199	$ 1,0\rangle \leftarrow 1,1\rangle_{+}$	0.185	0.186	0.013
16	B	8059.021	0.282	$ 0,0\rangle \leftarrow 1,1\rangle_{+}$	0.265	0.077	0.000
17	B	8059.204	0.465	$ 2,2\rangle_{+} \leftarrow 1,0\rangle$	0.461	0.031	0.048
18	B	8059.387	0.648	$ 2,2\rangle_{+} \leftarrow 1,1\rangle_{+}$	0.652	0.052	0.029
19	B	8059.503	0.763	$ 2,2\rangle_{-} \leftarrow 1,1\rangle_{-}$	0.767	0.026	0.030
20	B	8059.537	0.798	$ 2,2\rangle_{-} \leftarrow 1,1\rangle_{+}$	0.795	0.015	0.039
21	A	8060.838	2.099	$ 1,1\rangle_{\pm} \leftarrow 2,1\rangle_{\pm}$	2.099	1.000	1.000
22	B	8061.116	2.377	$ 1,0\rangle \leftarrow 2,1\rangle_{\pm}$	2.350	0.238	0.051
23	B	8061.145	2.406	$ 0,0\rangle \leftarrow 2,1\rangle_{\pm}$	2.408	0.190	0.360
24	B	8061.745	3.006	$ 2,0\rangle \leftarrow 2,2\rangle_{-}$	3.023	0.037	0.014
25	B	8061.824	3.085	$ 2,0\rangle \leftarrow 2,2\rangle_{+}$	3.114	0.014	0.020
26	B	8062.292	3.553	$ 2,0\rangle \leftarrow 0,0\rangle$	3.537	0.195	0.237
27	B	8062.487	3.747	$ 2,0\rangle \leftarrow 1,1\rangle_{-}$	3.737	0.190	0.236
28	C	8064.667	5.928	$ 2,0\rangle \leftarrow 2,1\rangle_{\pm}$	5.908	0.034	0.018

^aSee Fig. 9.

^b $\Delta\tilde{\nu}$ is the relative position referred to 8058.739 cm^{-1} , which is the origin of the $Q_2(1)$ transition.

^cTerm value differences obtained from this assignment. See also Fig. 10.

^dRelative values were obtained by setting the value for the strongest component (21) to 1.

^eCalculated from the transition dipole moments multiplied by the Boltzmann factor of the lower state. Transition dipole moments were calculated by T.J. Byers (private communication).

^fNo experimental value due to overlap with other transitions.

^gSum of the values for transition 5 and 6.

tion is roughly $8 \times \Gamma_{\text{EQQ}}$, when we assume that the EQQ interaction strongly dominates the orthohydrogen pair splitting pattern, and neglect any difference in temperature dependence of Γ_{EQQ} in the upper and lower states. We can therefore take the spacing between the two sharp components of this double transition to be a direct measure of the Γ_{EQQ} constant and study its behavior under temperature changes. In Fig. 14 the spacing $\Delta\tilde{\nu}$ is plotted versus the temperature. Again we find a rather smooth curve, which means that the determination of this value is precise enough to allow a quantitative analysis. This analysis will be discussed in Sec. IVC in some greater detail.

IV. ANALYSIS

A. The $Y_1(0)$ transition

As described in Sec. III A there is an unusually large discrepancy between the experimental line position of the

$Y_1(0)$ transition and its prediction from the modified Dunham model. In this model the assumption was made that the rovibrational term values of a hydrogen molecule in a solid hydrogen crystal can be expressed by a Dunham expansion series, as they can for the free molecule, employing Dunham coefficients with some additive correction terms. These correction terms can be reduced to a small number of dimensionless parameters μ_n where n accounts for the n th-order contribution of the leading terms of the isotropic intermolecular interaction. In their publication Van Kranendonk and Karl¹² present the result of an analysis in which they have used then available IR and Raman spectral data in order to fit numerical values of μ_1 and μ_2 . Their result was $\mu_1 = 0.03$ and $\mu_2 = -0.005$. The quality of this fit can be seen in Table III where most of the transitions listed were originally not included in the fit and are therefore predictions. The standard deviation for 15 selected line positions is 2.13 cm^{-1} . We repeated this fitting procedure including all the selected tran-

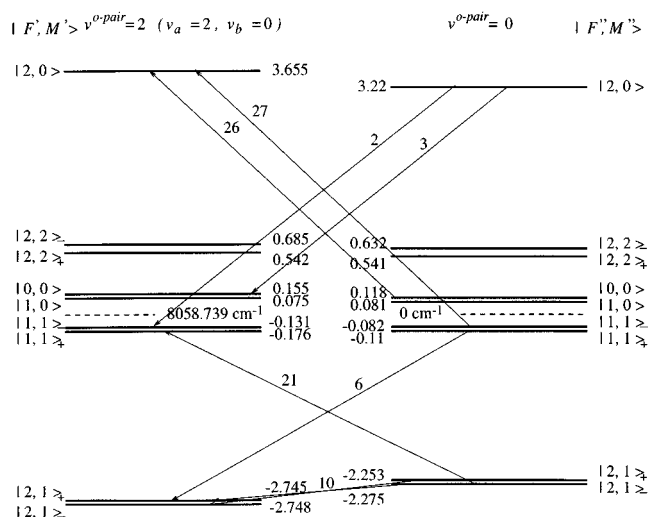


FIG. 10. Term diagram and the strongest orthohydrogen pair transitions associated with the $Q_2(1)$ transition. Transition labels are identical with those of Fig. 9. Numerical values are in cm^{-1} .

sitions in that table. Our selection criterion was that the lines in question should be single transitions that are neither shifted nor broadened by any vibron or roton propagation in order to account only for the isotropic single molecule interaction potential. The result of this new fit was $\mu_1 = 0.0408$ and $\mu_2 = -0.0179$. The resulting line positions are shown in Table VII where the standard deviation is now 1.10 cm^{-1} . The residual for the $Y_1(0)$ transition was reduced from 5.79 cm^{-1} to 2.73 cm^{-1} , but several other deviations are unsatisfactorily large. We believe that the assumptions made in this two-parameter model do not permit better predictions.

B. Thermal shift of line positions

Spectral shifts of sharp transitions upon variation of the temperature are due to thermal contraction of the crystal because all effects that contribute to the infrared spectrum of solid hydrogen depend on intermolecular forces and thus on the intermolecular separation R . As outlined in Ref. 18 the thermal contraction of solid hydrogen at normal pressure can be treated by a simple first-order perturbation calculation

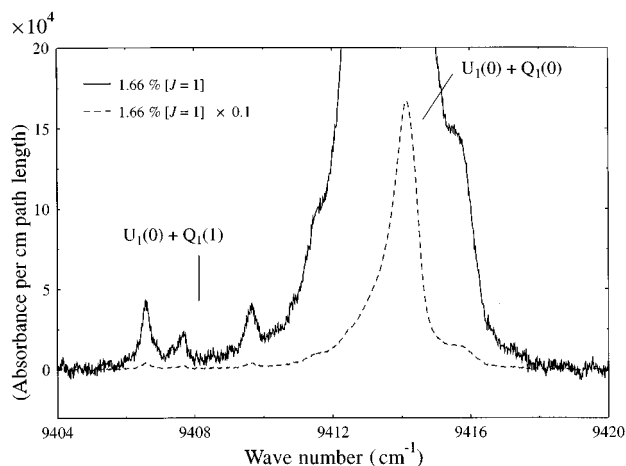


FIG. 11. The $U_1(0) + Q_1(1)$ and $U_1(0) + Q_1(0)$ transitions of solid hydrogen.

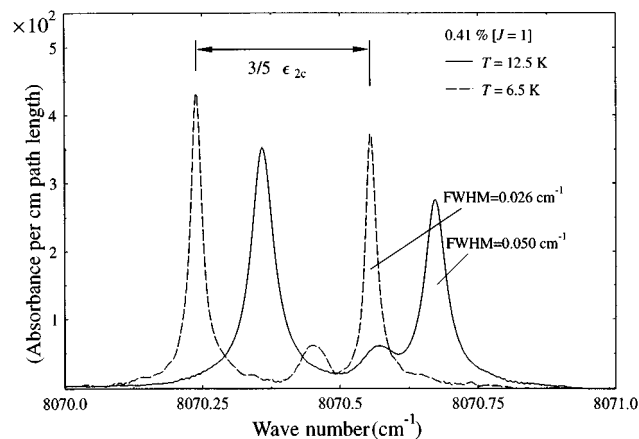


FIG. 12. Effect of temperature on the $Q_2(0)$ transition of solid parahydrogen.

since the change of R between 0 K and the triple-point temperature is only about 0.36% of its value. The intermolecular distance is of course connected with the molar volume by a third power law, which suggests looking at the temperature variation of the molar volume of solid hydrogen in order to study spectral shift effects. The first reliable measurements of this molar volume were performed by Krupskii, Prokhvatilov, and Shcherbakov²⁷ and were also reported in the book of Souers.²⁸ Their analysis yielded a simple power law for the molar volume of solid hydrogen of the form

$$\delta V(T) = V(T) - V(0) = 2.233 \times 10^{-6} T^{4.424} \text{ cm}^3/\text{mol}. \quad (4.1)$$

Consequently the thermal variation of the line positions should be of a similar form:

$$\delta \tilde{\nu}(T) = \tilde{\nu}(T) - \tilde{\nu}(0) = \left(\frac{\partial \tilde{\nu}}{\partial V} \right) \delta V(T) = \text{const} \times T^{4.424}. \quad (4.2)$$

Here the factor $\partial \tilde{\nu} / \partial V$ should be a constant, given by the R dependence of the intermolecular potential causing the deviation of the energy levels of solid hydrogen from those of the isolated molecule. In analogy to Eq. (4.2) we used the

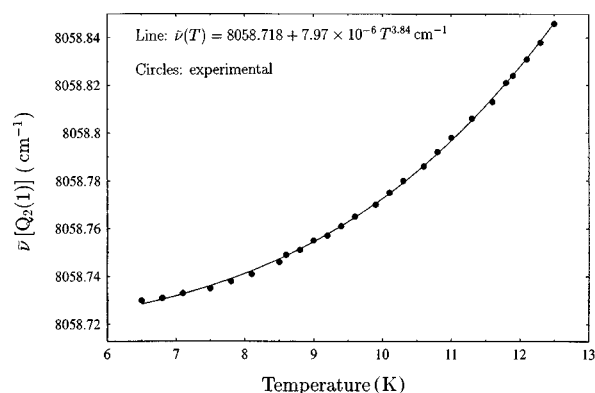


FIG. 13. Variation of the line position of the $Q_2(1)$ transition of solid hydrogen with temperature.

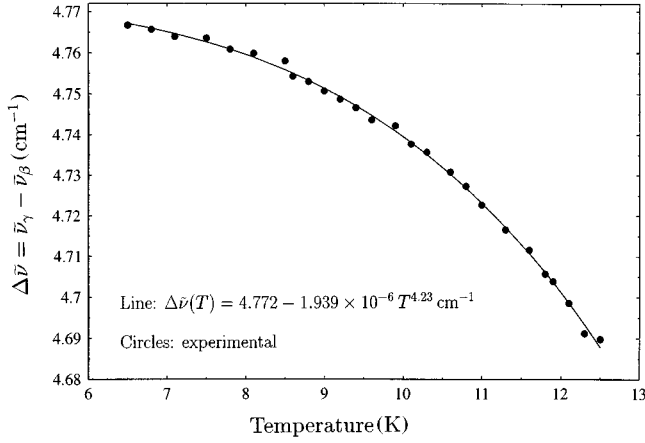


FIG. 14. Thermal shift of the wave number interval $\Delta\tilde{\nu}$ between the components γ and β of the $Q_1(1) + Q_1(1)$ double transition of solid hydrogen.

line positions of several transitions from the observed first overtone spectrum to fit the parameters a , b , and $\tilde{\nu}(0)$ of the empirical equation

$$\tilde{\nu}(T) = \tilde{\nu}(0) + a T^b. \quad (4.3)$$

The results of these fits are listed in Table VIII. We did not use all observable transitions because some of them were either too weak to produce accurate line positions or not symmetric. For example, the parameters obtained for a weak transition such as $U_2(0)$ have a much higher uncertainty than those of a strong transition such as $Q_2(0)$, as can be seen in Table VIII.

According to Eq. (4.2) the exponent b of the temperature should be 4.424 for all transitions. However, from Table VIII it is obvious that the adjusted values of this exponent are

TABLE VII. Rovibrational transitions of solid hydrogen reproduced with a modified Dunham model: New fit.

Transition	ν_{obs} (cm^{-1})	ν_{calc}^a (cm^{-1})	$\nu_{\text{obs}} - \nu_{\text{calc}}$ (cm^{-1})
$U_0(0)$	1167.12	1166.12	1.00
$W_0(0)$	2410.54	2409.39	1.15
$W_0(1)$	3063.48	3062.24	1.24
$Y_0(0)$	4044.18	4043.77	0.41
$Q_1(1)$	4146.51	4146.20	0.31
$S_1(1)$	4704.44	4702.90	1.54
$U_1(0)$	5261.28	5260.39	0.89
$U_1(1)$	5684.61	5683.88	0.73
$W_1(0)$	6441.81	6441.74	0.07
$W_1(1)$	7055.37	7056.07	-0.70
$Y_1(0)$	7991.71	7994.44	-2.73
$Q_2(1)$	8058.72	8058.39	0.33
$Q_2(0)$	8070.44	8069.75	0.69
$U_2(0)$	9122.21	9123.54	-1.33
$Q_3(0)$	11758.73	11758.38	0.35

^aCalculated from the modified Dunham model, Van Kranendonk and Karl (Ref. 12). The parameters $\mu_1 = 0.0408$ and $\mu_2 = -0.0179$ were adjusted using all listed transitions.

significantly lower and lie between 3.53 and 4.096. It is not possible to state whether this disagreement is due to experimental errors larger than estimated, or failure of one of our assumptions. For example, wall effects are not considered.

C. Thermal shift of Γ_{EQQ}

As can be seen in Fig. 14 we can analyze the temperature variation of the electric quadrupole-quadrupole coupling constant Γ_{EQQ} averaged over $v=0$ and $v=1$. We have fitted an empirical equation of the form of Eq. (4.3) to these data and find that the thermal variation of Γ_{EQQ} can be expressed by

$$\Gamma_{\text{EQQ}}(T) = [0.5966(1) - 2.4(7) \times 10^{-7} T^{4.23(11)}] \text{ cm}^{-1}. \quad (4.4)$$

We note that here the exponent of the temperature is closer to the expected value of 4.424 as in Eq. (4.2). But what is more interesting in this case is the total change $\Delta\Gamma_{\text{EQQ}}$ of Γ_{EQQ} when the temperature is raised from 6 to 12 K. From our data we find

$$\frac{\Delta\Gamma_{\text{EQQ}}}{\Gamma_{\text{EQQ}}} = -0.014(2) \quad (6 \rightarrow 12 \text{ K}). \quad (4.5)$$

Since the Γ_{EQQ} constant has a well-known dependence on the intermolecular distance, which is R^{-5} ,¹³ while the molar volume V is proportional to R^3 , there is a simple relation between the relative changes of Γ_{EQQ} and V :

$$\frac{\delta\Gamma_{\text{EQQ}}}{\Gamma_{\text{EQQ}}} = -\frac{5}{3} \frac{\delta V}{V}. \quad (4.6)$$

When using the numerical data for the change of the molar volume of solid parahydrogen from Ref. 27 we find for the same temperature interval of 6 to 12 K

$$-\frac{5}{3} \frac{\Delta V}{V}(\text{para-}H_2) = -0.0092, \quad (4.7)$$

which is about 35% lower than the observed relative change of Γ_{EQQ} of Eq. (4.5). However, when using the data for normal hydrogen containing 75% orthohydrogen we find

$$-\frac{5}{3} \frac{\Delta V}{V}(\text{normal-}H_2) = -0.0125, \quad (4.8)$$

which comes much closer to the observed value. Unfortunately there are no thermal expansion data available for pure orthohydrogen. The interpretation of this result is that the two orthohydrogen molecules that are responsible for the EQQ splitting seem to behave as part of an orthohydrogen crystal rather than a part of a parahydrogen crystal as far as the temperature variation of their distance is concerned.

D. Thermal shift of ϵ_{2c}

As described in Sec. III D 1 the crystal field splitting parameter ϵ_{2c} for the $v=2$ excited state can be determined from the line position difference of the two strong components of the $Q_2(0)$ transition. Since this parameter also de-

TABLE VIII. Thermal shift parameters for selected transitions of solid hydrogen.

Transition	$\tilde{\nu}(0)$ (cm^{-1})	a ($\text{cm}^{-1} \text{K}^{-b}$)	b
$Q_1(0)$ ^a	4149.6896	2.964×10^{-6}	4.096
$Q_2(1)$	8058.7180(8)	$7.9 (1.2) \times 10^{-6}$	3.84(6)
$Q_2(0)$	8070.4438(9)	$8.4 (1.4) \times 10^{-6}$	3.82(6)
$Q_1(1) + Q_1(1)$	8293.001(1)	$7.2 (1.2) \times 10^{-6}$	3.94(6)
$S_2(0)$	8387.340(1)	$6.0 (1.2) \times 10^{-6}$	4.03(8)
$U_2(0)$	9122.210(3)	$7.2 (4.6) \times 10^{-6}$	3.86(25)
$Q_2(0) + U_0(0)$	9237.346(3)	$1.9 (0.8) \times 10^{-5}$	3.53(15)

^aFrom Ref. 18.

depends on the intermolecular distance it should show a characteristic thermal shift. Figure 15 shows the variation of ϵ_{2c} with temperature. The solid line marks a fitted empirical curve given by

$$\epsilon_{2c}(T) = [-0.5300(2) + 8.3(4.7) \times 10^{-7} T^{3.5(2)}] \text{ cm}^{-1}. \quad (4.9)$$

According to Ref. 13 the parameter ϵ_{2c} is proportional to R^{-8} and, thus, the relative change of ϵ_{2c} should be

$$\frac{\delta \epsilon_{2c}}{\epsilon_{2c}} = -\frac{8}{3} \frac{\delta V}{V}, \quad (4.10)$$

which has a value of -0.0147 for solid parahydrogen over the temperature interval 6 to 12 K using the molar volume data of Ref. 27 again. However, we observe a value of only

$$\frac{\Delta \epsilon_{2c}}{\epsilon_{2c}} = -0.0098 \quad (6 \rightarrow 12 \text{ K}). \quad (4.11)$$

Here we cannot offer a simple explanation of the discrepancy between the model and the experimental result.

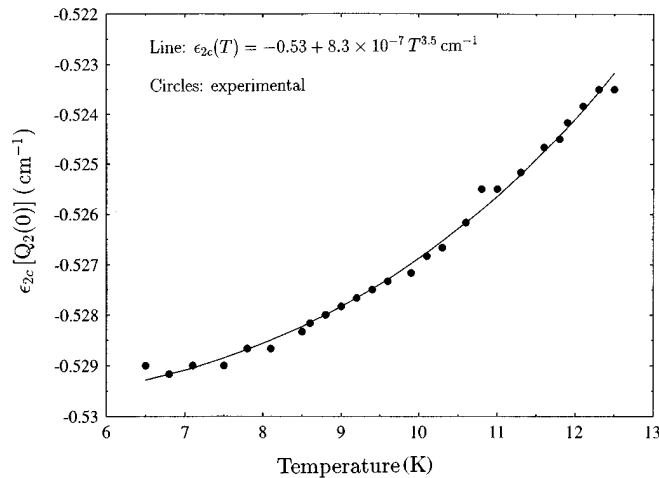


FIG. 15. Thermal shift of the crystal field splitting parameter ϵ_{2c} for the $\nu=2$ vibrationally excited state as deduced from the splitting of the $Q_2(0)$ transition of solid hydrogen.

V. CONCLUSION

In this work we have presented spectroscopic results in the first overtone region of solid hydrogen using a Fourier-transform spectrometer. This was achieved by enhancing the optical path length through the crystal to a large value, by preparing samples with low orthohydrogen impurity levels, and by investigation with high spectral resolution. This resolution was optimized in the sense that it was not so low as to hide narrow absorption features but not so high as to waste sensitivity either. Except for the very narrow $Y_1(0)$ transition, all observed features were limited in resolution by inherent crystal effects but not by the instrument. We believe this to be the first high-resolution investigation of the whole spectral region of $7900 - 10\,000 \text{ cm}^{-1}$ in solid hydrogen. The sensitivity of our measurements was such that we were able to observe absorption features as weak as $10^{-21} \text{ cm}^3 \text{ s}^{-1}$ (orthohydrogen features as weak as $10^{-19} \text{ cm}^3 \text{ s}^{-1}$), and when reducing the spectral range by a narrow band-pass filter, even $10^{-23} \text{ cm}^3 \text{ s}^{-1}$.

Due to these experimental conditions we could observe new transitions, and reveal new and interesting properties of known transitions. Among the new transitions the most interesting is undoubtedly the $Q_1(0) + Q_1(0)$ double transition because it can only be explained by an induction mechanism that has never been considered previously in absorption spectroscopy. It is planned to be presented in a separate publication. Many of the orthohydrogen transitions reported here were previously observed only in normal hydrogen at an orthohydrogen impurity level of 75% and were therefore strongly broadened and overlapped with neighboring transitions. In this work all these transitions were seen as individual absorption features.

We report here the observation of satellite structure due to orthohydrogen pair interactions in the first overtone region. For the strong $Q_2(0)$ transition this fine structure was studied in detail, which revealed more information than the corresponding structure for the $Q_1(0)$ transition because the individual fine structure peaks are narrower and less overlapped here. The corresponding results for the $Q_2(1)$ transition complement the laser spectroscopy data for the $Q_1(1)$ transition.^{22,29}

Finally we show that Fourier-transform spectra of thermally shifted absorption features in solid hydrogen can be recorded with sufficient precision to obtain information concerning the thermal expansion.

ACKNOWLEDGMENTS

This work was supported by the Deutsche Forschungsgemeinschaft, the Fonds der Chemischen Industrie, and a Max-Planck Research Award. Parts of the experimental equipment were financed by the CNRS, France and The Ohio State University due to earlier joint projects. Preliminary re-

sults obtained by R. Steinhoff were the basis of the extensive measurements reported here. We gratefully acknowledge the help of S. Klee and G. Mellau in handling the Bruker IFS 120 HR interferometer. We finally wish to thank T. Oka and Y. Zhang for helpful discussions and T. J. Byers for providing her calculations prior to publication.

-
- ¹R. A. Steinhoff, B. P. Winnewisser, and M. Winnewisser, *Phys. Rev. Lett.* **73**, 2833 (1994).
- ²C. Y. Kuo, M. M. F. Vieira, R. J. Kerl, and C. K. N. Patel, *Phys. Rev. Lett.* **50**, 256 (1983).
- ³H. P. Gush, W. F. J. Hare, E. J. Allin, and H. L. Welsh, *Can. J. Phys.* **38**, 176 (1960).
- ⁴S. S. Bhatnagar, E. J. Allin, and H. L. Welsh, *Can. J. Phys.* **40**, 9 (1962).
- ⁵K. Narahari Rao, J. R. Gaines, T. K. Balasubramanian, and R. D'Cunha, *Acta Phys. Hung.* **55**, 383 (1984).
- ⁶T. Oka, *Annu. Rev. Phys. Chem.* **44**, 299 (1993).
- ⁷R. A. Steinhoff, K. V. S. R. Apparao, D. W. Ferguson, K. Narahari Rao, B. P. Winnewisser, and M. Winnewisser, *Can. J. Phys.* **72**, 1122 (1994).
- ⁸D. P. Weliky, T. J. Byers, K. E. Kerr, T. Momose, R. M. Dickson, and T. Oka, *Appl. Phys. B* **59**, 265 (1994).
- ⁹R. M. Dickson and T. Oka, *J. Phys. Chem.* **99**, 2617 (1995).
- ¹⁰J. V. Kranendonk, *Can. J. Phys.* **38**, 240 (1960).
- ¹¹V. F. Sears and J. V. Kranendonk, *Can. J. Phys.* **42**, 980 (1964).
- ¹²J. V. Kranendonk and G. Karl, *Rev. Mod. Phys.* **40**, 531 (1968).
- ¹³J. V. Kranendonk, *Solid Hydrogen* (Plenum Press, New York, 1983).
- ¹⁴G. Varghese, R. D. G. Prasad, and S. Paddi Reddy, *Phys. Rev. A* **35**, 701 (1987).
- ¹⁵S. Y. Lee, Ph.D. Dissertation, The Ohio State University, Columbus, Ohio, 1987.
- ¹⁶R. Steinhoff, K. V. S. R. Apparao, D. W. Ferguson, K. Narahari Rao, B. P. Winnewisser, and M. Winnewisser, *Appl. Opt.* **32**, 6577 (1993).
- ¹⁷T. Oka, *J. Low Temp. Phys.* **22**, 96 (1996).
- ¹⁸K. E. Kerr, T. Momose, D. P. Weliky, C. M. Gabrys, and T. Oka, *Phys. Rev. Lett.* **72**, 3957 (1994).
- ¹⁹R. A. Steinhoff, Ph.D. Dissertation, Justus-Liebig-Universität, Giessen, Germany, 1995.
- ²⁰W. N. Hardy, A. J. Berlinsky, and A. B. Harris, *Can. J. Phys.* **55**, 1150 (1977).
- ²¹A. B. Harris, A. J. Berlinsky, and W. N. Hardy, *Can. J. Phys.* **55**, 1180 (1977).
- ²²M. C. Chan, Ph.D. Dissertation, The University of Chicago, Chicago, IL, 1991.
- ²³R. M. Dickson, T. J. Byers, and T. Oka, *J. Low Temp. Phys.* **102**, 241 (1996).
- ²⁴T. J. Byers, Ph.D. Dissertation, The University of Chicago, Chicago, IL, 1995.
- ²⁵F. Schreier and B. Schimpf, *FITMAS Manual, DLR* (Deutsche Forschungsanstalt für Luft- und Raumfahrt, Oberpfaffenhofen, Germany, 1995).
- ²⁶J. W. C. Johns, *Mikrochim. Acta [Wien]* **III**, 171 (1987).
- ²⁷I. N. Krupskii, A. I. Prokhvatilov, and G. N. Shcherbakov, *Fiz. Nizk. Temp.* **9**, 83 (1983) [*Sov. J. Low Temp. Phys.* **9**, 42 (1983)].
- ²⁸P. C. Souers, *Hydrogen Properties for Fusion Energy* (University of California Press, Berkeley, 1986).
- ²⁹Y. Zhang and T. Oka (private communication).